

Formation and structure of the potassium complex of valinomycin in solution studied by Raman optical activity spectroscopy†

Shigeki Yamamoto,^{*ab} Michal Straka,^a Hitoshi Watarai^b and Petr Bour^{**a}

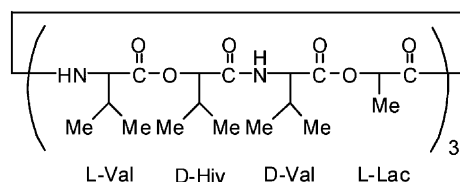
Received 16th February 2010, Accepted 4th June 2010

DOI: 10.1039/c003277h

The formation and structure of the potassium complex with valinomycin in solution were studied by means of Raman and Raman optical activity (ROA) spectroscopy. The complexation caused significant spectral changes, particularly in the region 1200–1400 cm⁻¹. The experimental spectra were interpreted using first principles computations. A complete computational conformational search combined with the spectral analysis revealed the arrangement of the isopropyl side chains in the complex. From a total of 6579 unique conformers two predominant ones were confirmed in the solution by ROA. A third one was predicted theoretically, but its population in the experiment could be estimated only roughly. The most populated conformer does not exhibit C₃ symmetry, and is different from that present in the crystal and the NMR-derived structure. Molecular dynamics techniques were used to estimate the molecular flexibility and its effect on the spectra. Density functional computations and Cartesian coordinate transfer (CCT) techniques provided the ROA and Raman spectral shapes and intensities well comparable with the experiment. The polar solvent (methanol) environment modeled with a polarizable continuum model (PCM) leads to rather minor changes in the conformer populations and vibrational properties as compared to vacuum computations, due to the hydrophobic character of the complex. Additional computational experiments suggest that the vibrational interactions determining the ROA spectra are quite local, which contributes to the good spatial resolution of the method. A reduction of the noise in the experimental spectra as well as increased precision of the simulations is desirable for the further exploration of the potential of the ROA spectroscopy for biomolecular studies in the future.

Introduction

Valinomycin is a neutral ionophore produced by the bacterium *Streptomyces fulvissimus*. It has a highly selective ability to make a complex with the potassium ion.^{1–3} Its conformational flexibility is crucial for the biological functions, facilitating the capture of the metal, its transport across the lipid cell membrane, and the release of the ion. In addition to the induction of the ionic permeability, valinomycin exhibits strong microbial activity.⁴ The molecule is a cyclic depsipeptide made of L- and D-valine (Val) amino acids, D- α -hydroxyisovaleric (Hiv) and L-lactic (Lac) acids, with a three-times repeating structure:



In spite of the polar amide and ester moieties, the peptide is not in significant amounts soluble in water, due to the hydrophobic methyl and isopropyl side chains.

The side chain conformation itself is probably not important for the biological role, although it may be changed by interactions with aromatic ions, diminishing the potassium binding specificity during the transfer.⁵ However, the strong ROA signal of the isopropyl residues makes the valinomycin molecule an ideal model system for testing the sensitivity of the spectra to fine structural features. Other optical methods do not provide sufficient information about the side chain conformation. The isopropyl average positions in solution can be deduced from indirect spin–spin coupling constants,^{6–10} but individual angles for particular residues cannot be determined by NMR due to the fast conformational exchange. There are indications that the crystal structure^{11–13} of valinomycin is at least slightly different from that in solution.⁶ Unlike for NMR, the ROA spectrum is an algebraic sum of conformer subspectra, so that it can provide welcome complementary information

^a Institute of Organic Chemistry and Biochemistry, Academy of Sciences, 166 10 Prague, Czech Republic. E-mail: aporoa@gmail.com, bour@uochb.cas.cz

^b Department of Chemistry, Graduate School of Science, Osaka University, Toyonaka, Osaka 560-0043, Japan

† Electronic supplementary information (ESI) available: Table S1 with vibrational mode assignments, Tables S2–S4 with computational details of the conformer search, Fig. S1 with relative energies of conformers, Fig. S2 with lowest-energy conformer, Fig. S3 with simulated ROA spectra, Fig. S4 with results from MD simulations, and Fig. S5 with ROA CID calculated and experimental ratios. Functional tests (Fig. S6), explicit solvation (Fig. S7–S8) and the B3PW91 decomposition (Fig. S9) are also documented. See DOI: 10.1039/c003277h

about the molecular structure and dynamics in solution. Supposedly, the ROA signal of a weakly interacting solvent is either small or always averaged over a vast number of configurations, reasonably well represented by the continuum solvent model. For smaller dipeptides, the conformer populations obtained by ROA were shown to be equivalent to those obtained by NMR spectroscopy.¹⁴

The valinomycin structure including its complexes was also studied by other methods, including, for example, unpolarized Raman spectroscopy,^{15–17} infrared absorption (IR),¹⁸ optical rotatory dispersion (ORD),⁷ and electronic and vibrational circular dichroism (ECD, VCD).^{3,19} In particular, the VCD technique provides important knowledge about the peptide backbone, but the side chain VCD signal is too weak.¹⁷

The valinomycin molecule can adopt different shapes. If crystallized from non-polar solvents, all six NH groups of the amide bonds are involved in intermolecular hydrogen bonding.^{11,12} In a crystal of the K^+ -complex valinomycin adopts the so called bracelet conformation where the six ester carbonyl groups point to an inward cavity where they bind to the potassium cation.¹³ This structure is additionally stabilized by the intramolecular hydrogen bonds between amide carbonyl and NH groups. Such saturation of the polar molecular residues contributes to the hydrophobic character of the complex and enables the cross-membrane transport.²

The ROA spectrum measures the difference in the Raman scattering of right- and left circularly polarized light.²⁰ Since its discovery²¹ the technique has brought important advantages into the spectroscopic investigation of biomolecular systems. Unlike the unpolarized Raman scattering, ROA bands can be both positive and negative, which makes their assignment and identification easier. Additionally, the polarized spectra are in general more sensitive to the conformation. Unlike VCD²² and IR, the ROA spectra are measured using visible light, which is more compatible with the natural aqueous solvent environment and conventional optics. The vibrational domain also provides more and better resolved transitions than the electronic excited states seen in ultraviolet and visible absorption (UV-vis) and circular dichroism (CD).²³ The vibrational interactions are fairly local, sensitive to conformation of individual molecular parts,²⁴ although for small molecules the backbone contributes more significantly.²⁵ The locality can be further explored by labeling of stable isotopes.²⁶ Lately, we have shown that inhomogeneous Raman and ROA band widths are directly related to molecular flexibility and dynamics.^{27,28}

Interpretations of the ROA spectra are largely dependent on the quantum-chemical computations.^{29,30} The ROA intensity simulations have become origin-independent and thus significantly more reliable since the introduction of the gauge-invariant atomic orbitals (GIAO).^{31,32} An analytical implementation within the density-functional theory (DFT) enabled extended ROA applications to larger molecules.³² Still, the computations of the intensity tensors were hindered by a numerical differentiation, an obstacle that was removed only lately.^{33,34} Nowadays, computations of ROA intensities can be done with approximately the same effort as for the Raman intensities with popular software packages.^{35,36} Nevertheless, the fine splitting of vibrational energy levels and the second-order

intensity response properties determining the ROA spectrum require large basis sets and high-quality approximations,^{37,38} which become prohibitive for larger molecules. Direct ROA simulations for peptides containing up to ten alanine residues have been reported so far.³⁹

For more sizable systems, such as the valinomycin molecule, or for higher accuracy the vibrational spectra can be conveniently generated by the Cartesian coordinate tensors transfer (CCT) techniques,⁴⁰ which provide results of nearly full *ab initio* quality.⁴¹ In CCT, the force field (second energy derivatives) and molecular property tensors are calculated at a high approximation level for smaller molecular fragments, and then transferred to the target molecules. For the ROA intensities, derivatives of the magnetic dipole-electric dipole (G') and electric quadrupole-electric dipole (A) polarizability tensors are needed, together with the usual dipolar polarizability (α). The CCT methodology has successfully been used for simulations of IR and VCD spectra of peptides,⁴² proteins,⁴³ and nucleic acids.⁴⁴ Regularly, CCT for ROA is used to combine computational results obtained at various approximation levels,^{28,32} or to build up vibrational properties of larger molecules.⁴⁵ However, origin-dependence related problems^{20,46} encountered in the transfer of the ROA valinomycin properties introduced errors into the resultant intensities. Fortunately, relatively fast analytical computations of G' and A became available lately.^{33,34} Therefore, as a default, a rather unusual procedure is chosen in this study, where for smaller fragments the harmonic force field and polarizability (α) are calculated at a higher level, but the ROA tensors are calculated at once for the whole valinomycin molecule. This leads to a good numerical stability of the results, and the simulated spectra very well match the experimental observations.

For the CCT method being meaningful, the fragment structure must be kept close to that of the whole complex, while the higher-frequency vibrational modes need to be relaxed. This was enabled by the constrained normal mode optimization algorithm^{47,48} that previously provided results superior to the usual fixing of torsion angles in peptides and nucleic acids.^{49,50} The solvent influence is accounted for by the polarizable continuum model (PCM) based on the conductor-like solvent model (COSMO) of Klamt.⁵¹ The dielectric continuum solvent approximation has been previously criticized for strongly polar systems;^{52–55} however, as shown below, the influence of the environment on the spectroscopic valinomycin properties is rather modest, and PCM provides reasonable results in this case.

Involvement of explicit solvent molecules was not attempted for the spectra calculation due to the size of the system. It should be noted that for modeling of vibrational optical activity of more polar systems, explicit solvent is recommended for better description of the hydrogen bonding.^{52,53,56} In particular, peptide zwitterions are not only unstable in vacuum, but their conformation may be stabilized by solvent, which is difficult to reproduce with implicit models.^{57,58} Dielectric models also often fail to reproduce the effect of the hydrogen bonding on vibrational frequencies.^{54,55} However, these effects are limited for the hydrophobic valinomycin–potassium complex. For example, molecular dynamics modeling suggests that only the amide oxygen atoms may strongly interact with

methanol, without significant perturbation of the structure and spectra.

Methods

Experimental

Valinomycin (of $\geq 90\%$ purity) was purchased from Sigma, and recrystallized twice from methanol (99.9%, Acros Organics). The concentration of valinomycin in the methanol solutions for the measurement was 0.12 M. The potassium–valinomycin complex was prepared by dissolving molar equivalents of KCl (Fluka Corp.) and valinomycin in methanol. Back-scattered circular polarized ROA spectra were measured on a home-made instrument at the University of Fribourg. A dual arm light collection arrangement with optical fiber bundles enabled the simultaneous detection of right and left circularly polarized Raman light.⁵⁹ The correction scheme using half-wave retarders reduced the deterministic error in the ROA spectrum.⁶⁰ The spectra were collected with the excitation wavelength of 532 nm, 7 cm⁻¹ resolution, laser power at the sample 400 mW, and temperature of 300 K. The sample was held in a small drum cell with black Teflon walls and two glass windows; the sample volume was ~ 35 μL . In order to reduce the fluorescence background of residual impurities, the sample was irradiated by laser light over 5 h before measurement. In order to check reproducibility, the measurement of each sample was repeated three times with slightly different positions of the laser focus; the sum of the three spectra is reported. The solvent peaks and fluorescence background were subtracted from the Raman spectra; for ROA a third-order nine-point Savitzky-Golay smoothing was applied. The experimental intensities are presented in units of the total number of electrons detected in the CCD camera.

Conformation search of the potassium–valinomycin complex

Starting X-ray geometry¹¹ was downloaded from the Cambridge structural database (<http://www.ccdc.cam.ac.uk>). Using the MCM software⁶¹ nine isopropyl torsion angles (see Fig. 1 for the definition) were systematically varied as -60 , 60 and 180° , so that $3^9 = 19\,683$ conformers were generated. Exploring the periodicity of the molecular sequence, 6579 unique structures were selected for optimization of the geometry by energy minimization within the Gaussian program.³⁵ The PM3⁶² and AM1⁶³ semiempirical methods were used to evaluate the equilibrium energies of all conformers. Because accurate potassium parameters were not available for these computations, the K⁺ ion was replaced by proton (H⁺) and the proton–oxygen distances in the complex were fixed to 2.81 Å. All other coordinates were fully relaxed during the optimizations.

Twelve lowest-energy AM1 conformers thus obtained were optimized at the BPW91⁶⁴/6-31G** level with and without the methanol environment. The Gaussian version of the COSMO⁵¹ model (CPCM) was used for the solvent. For a limited number of conformers the B3LYP⁶⁵ functional and 6-311++G** basis were used. All the higher-level DFT computations were performed with the proper K⁺ ion without any geometrical constraints. As an independent test of the reliability of the

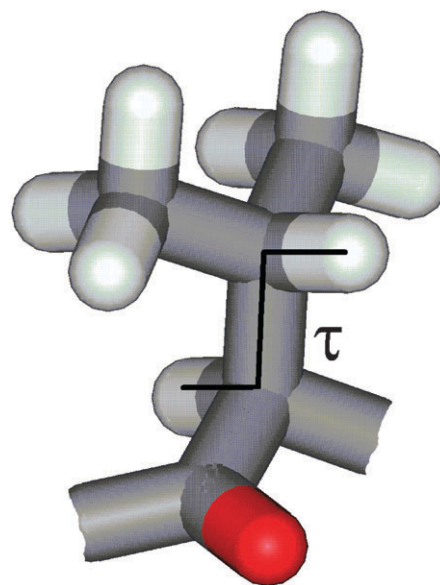


Fig. 1 Definition of the torsion angle $\tau = \angle(\alpha\text{H}, \alpha\text{C}, \beta\text{C}, \beta\text{H})$ determining the isopropyl positions.

computations, equilibrium structures and energies of all 27 conformers exhibiting the C₃ symmetry were calculated at the HF/3-21, BPW91/6-31G**, BPW91/PCM(MeOH)/6-31G**, B3PW91⁶⁶/PCM(MeOH)/6-31G**, and B3LYP/6-31G** approximation levels. The HF/3-21 and BPW91/6-31G** computations were also performed with the Grimme van der Waals dispersion correction,^{67–69} which, however, did not cause significant changes in the conformer ordering.

Molecular dynamics

The Tinker program package⁷⁰ with the Amber99 force field⁷¹ was used to estimate the side chain flexibility, and its subsequent influence on the spectra. The K⁺-valinomycin complex was placed into a cubic periodic box of 30 Å a side, together with the methanol molecules. As an NVT ensemble (with 1 fs integration time step) the system was equilibrated for 20 ps at 1000 K, and annealed to 298 K for 300 ps. The annealed structure was allowed to evolve for 1500 ps. Because reliable force field parameters for the potassium ion bound to the peptide were not available, the distances between K⁺ and the six closest oxygen atoms¹¹ were kept fixed to 2.81 Å.

ROA and Raman spectra calculation

The spectra were generated for the fully optimized K⁺-valinomycin complexes described above, and also for free valinomycin conformers as obtained from the structural database.¹² In order to relax the higher-frequency modes in the free molecules, the geometries were partially optimized in the normal mode coordinates.^{47,48} Modes between $i300$ (imaginary) and 300 cm⁻¹ were kept constant, which led to minor changes of initial geometries only. For the optimized structures, harmonic force fields were calculated by the Gaussian³⁵ or Turbomole⁷² programs. Turbomole was used to reoptimize the structure and calculate the vibrational frequencies at the BP86/SVP(def2-TZVPP for potassium) level.

The performance of a broader family including newer functionals (M05,⁷³ M06,⁷⁴ M062X,⁷⁴ M06L,⁷⁵ B3LYP,⁶⁵ B3PW91)⁶⁶ was tested on the Raman spectra of a L-Lac-L-Val-D-Hiv-D-Val fragment bond to potassium, with the 6-311++G** basis set and the PCM(MeOH) model. The spectra were calculated using Gaussian for partially optimized geometries of the fragment, with torsional angles constrained to those in the valinomycin complex fully optimized at B3LYP/6-31G**/PCM(MeOH) level. However, no particular advantage of the newer functionals over the more common B3LYP method was observed, perhaps except for some spectral details better reproduced by B3PW91.

The ROA intensity tensors were obtained by Gaussian for the whole molecule at the HF/6-31G and HF/6-31** levels. Smaller fragments (*cf.* Fig. 2) were created from the target molecules and partially optimized in the normal mode coordinates with the parameters specified above. For the fragments, the harmonic force field and Raman intensity tensor (α) were calculated by Gaussian at the B3LYP/PCM(MeOH)/6-31++G** level, and transferred in the Cartesian coordinate to the whole valinomycin by the CCT program.^{40,76} The B3PW91⁶⁶ functional with the same basis set and solvent model was also used for comparison. The back-scattering Raman and ROA intensities were obtained as^{14,77,78} $I_{\text{Ram}} = 6 \sum_{i=1..3} \sum_{j=1..3} (7\alpha_{ij}\alpha_{ij} + \alpha_{ii}\alpha_{ii})$ and $I_{\text{ROA}} = \frac{48}{c} \sum_{i=1..3} \sum_{j=1..3} \left(3\alpha_{ij}G'_{ij} - \alpha_{ii}G'_{jj} + \omega_{\text{exc}} \sum_{k=1..3} \varepsilon_{ijk}\alpha_{il}A_{jkl}/3 \right)$, respectively, where c is velocity of light, ω_{exc} the laser frequency, and ε_{ijk} the antisymmetric unit tensor.

Lorentzian spectral shapes and temperature corrections were applied to generate the spectrum from individual peaks as $S(\omega) = I_{\text{Ram/ROA}} [1 - \exp(-\frac{\omega_i}{kT})]^{-1} \frac{1}{\omega_i} \left[4 \left(\frac{\omega - \omega_i}{\Delta} \right)^2 + 1 \right]^{-1}$, where

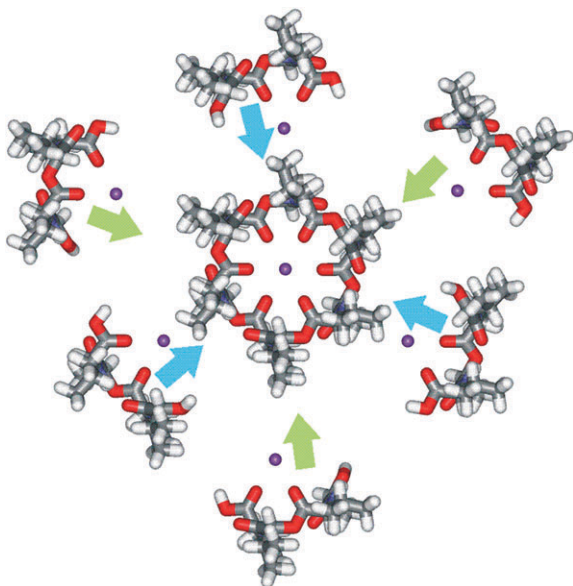


Fig. 2 Fragmentation of the valinomycin potassium complex used to generate a molecular force field and intensity tensors. Calculated (B3LYP/CPCM(MeOH)/6-31++G**) parameters for six partially overlapping smaller segments of two different sequences were transferred to the target molecule.

ω_i is the vibrational frequency, k the Boltzmann constant, T temperature, and $\Delta = 5 \text{ cm}^{-1}$. The computed spectra were adjusted by one scale factor (common to Raman and ROA) to the average experimental intensity, and individual frequencies were scaled according to experiment with the aid of the SC95 software.⁷⁹ Within SC95 and other simple scripts, the experimental ROA spectra were also decomposed into calculated subspectra of individual conformers, using the algorithm described elsewhere.^{14,30,80}

Results and discussion

The complex formation evidenced by ROA

Experimental ROA and Raman spectra of valinomycin in methanol in the absence and presence of the potassium ion are shown in Fig. 3 (left). The complexation is clearly reflected in the changes of the spectral shape. Generally, the free valinomycin exhibits fewer and broader peaks, especially at the lowest-wavenumber region ($150 \cdot \cdot 800 \text{ cm}^{-1}$). On the basis of the previous analyses,^{27,28,30,81,82} we can associate the broadening with the flexibility of the free peptide, which adopts a more elastic propeller form.¹² The ROA spectrum changes even more than the Raman scattering. However, some spectral features are modified only slightly under the complexation, such as the $1461/1447 \text{ cm}^{-1} +/ -$ couplet, where a third weak band appears at 1470 cm^{-1} for the complex. A similar couplet around 1335 cm^{-1} becomes narrower in the complex, but the principal ROA features seem to be conserved in both valinomycin forms down to about 900 cm^{-1} . Interestingly, the restricted conformational freedom in the complex does not lead to an increase of the ROA signal below 400 cm^{-1} , but the intensity is redistributed in this region. The different responses of various wavenumber ranges to the complexation can be explained by the locality of the higher-frequency vibrations, while the delocalized vibrational modes which are more sensitive to the change of the molecular shape have usually lower frequencies.

Further minor changes upon complexation can be seen through the entire frequency region both in Raman and ROA spectra. The ester carbonyl band at 1750 cm^{-1} in valinomycin shifts up to 1757 cm^{-1} in the complex, while the partially resolved amide I bands (1676 and 1657 cm^{-1}) are shifted down to 1662 cm^{-1} and 1646 cm^{-1} , which corresponds to the previous observation with ethanol as a solvent.¹⁵ The carbonyl band shifts were attributed to the interaction between the ester carbonyl and potassium ion, and to the resultant increase of the extent of hydrogen bonding at the amide carbonyl.¹⁵ The carbonyl stretch transitions could not be detected by ROA due to the limited sensitivity. In both spectral types intensity changes also in the amide III and hydrogen bending region ($1200\text{--}1400 \text{ cm}^{-1}$). These vibrations involve mixed NH and $C_\alpha H$ deformations⁸³ and are known to be sensitive to the geometry of peptides and proteins in ROA spectra.⁸⁴ The free valinomycin exhibits broad bands at 1300 and 1400 cm^{-1} , which become sharper peaks at 1318 cm^{-1} and 1338 cm^{-1} in the complex.

On the basis of the calculated spectra (right hand side of Fig. 3) and normal mode displacements, we could assign

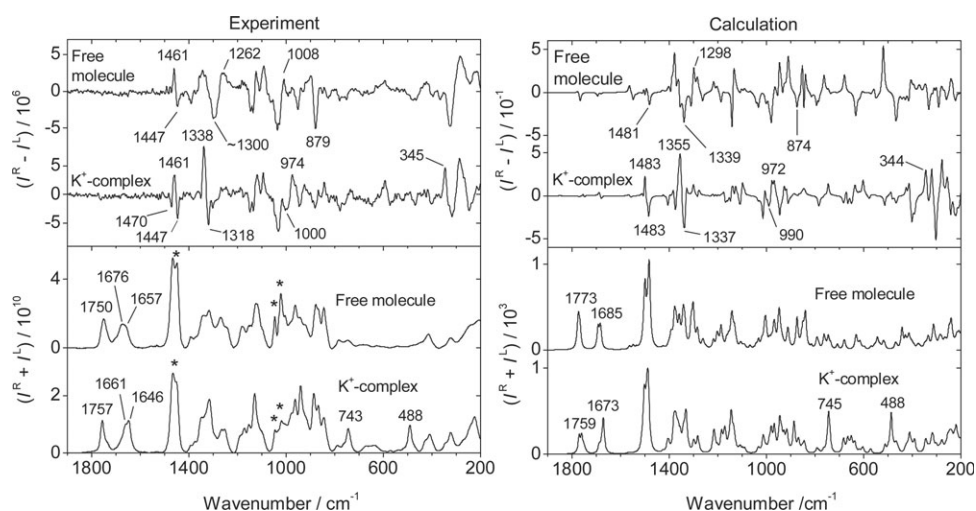


Fig. 3 The left part shows the experimental ROA (top) and Raman (bottom) spectra of free valinomycin and its potassium complex in methanol. On the right hand side, the corresponding simulated (B3LYP/6-31G**/CPCM(MeOH)/HF/6-31G) spectra are plotted. The asterisks at the experimental Raman spectrum indicate highly overlapped peaks that may be affected by the solvent.

most of the observed Raman and ROA bands (Tables S1 in the ESI)†, which mostly corresponds to earlier assignments.^{17,18} The region below 400 cm^{-1} , for example is dominated by soft modes, such as methyl torsions, skeletal deformations, and breathing of the peptide. The sharp ROA peak at 879 cm^{-1} (Raman at 874 cm^{-1}) of free valinomycin which becomes weaker in the complex stems from delocalized CC stretch and carbonyl carbon out of plane deviation.¹⁷ Raman intensities of the antisymmetric CH_3 bending at 1450 cm^{-1} (in-phase) and 1468 cm^{-1} (out-of-phase)^{17,18} may be obscured by the solvent bands. Previously, the Raman signal of these modes was found to be insensitive to conformational changes,¹⁷ which contrasts with the corresponding ROA signal variations. The $+/-$ ROA couplet (1461/1447 cm^{-1}) of free valinomycin becomes a $-/+/-$ w-shaped signal (1470/1461/1447 cm^{-1}) in the complex. The calculated ROA and spectral curves (Fig. 3, right) reproduce the most important changes observed under the complexation (characteristic complex Raman bands at 743/488 cm^{-1} , calculated at 745/488 cm^{-1} , ROA signal transition around 1335 cm^{-1} , etc.), although we could not reproduce many finer spectral features of the free molecule, due to its flexibility and a huge number of conformations given by the complicated dynamics in solution. On the other hand, for the complex, the analysis presented below reveals even more details about molecular structure.

Conformational search for the complex

The relative energy distribution of the 6579 conformers differing by positions of the isopropyl residues calculated at the AM1 level is plotted in Fig. 4. The PM3 method (not shown) gave very similar results. From the AM1 energy dependence, we can see that a relatively small number of structures can be populated at the room temperature (the Boltzmann quantum is about 0.6 kcal mol^{-1}). The lowest-energy geometry exhibits C_3 symmetry; however, other structures of this symmetry are distributed over the entire conformational space (see the red lines in Fig. 4), although they are somewhat clustered at the lowest- and highest-energy regions.

It is currently not affordable for us to obtain reliable estimates of the energies of all conformers at a higher computational level; however, for selected conformers the semiempirical AM1 and PM3 results correlate very well with the HF and DFT (B3LYP and BPW91) computations (Fig. S1 and Tables S2 and S3 in the ESI).† Whereas the semiempirical methods provide relative energies underestimated by about 50% in comparison with DFT, the relative ordering of conformers is preserved in the majority of cases. Neither the dielectric continuum PCM solvent correction, nor the larger 6-311++G** basis set (*cf.* right part of Fig. S1†) or the Grimme dispersion correction⁶⁷ (not shown) brought significant changes in the lowest-energy conformer ordering. The relative independence of the conformer ordering on the adopted computational method suggests that the conformational convenience is primarily driven by sterical geometrical factors rather than complicated rearrangements in electronic structure. The indifference to the

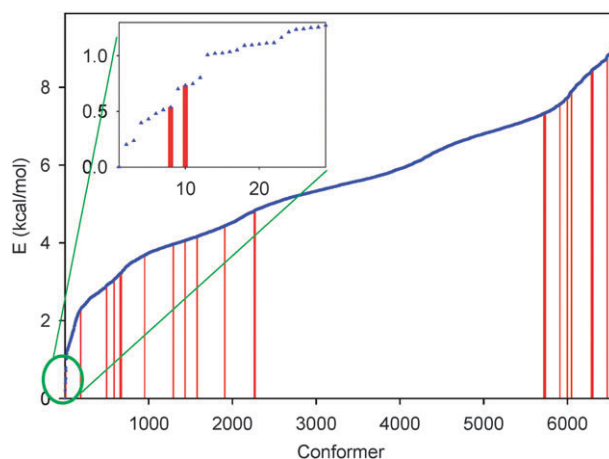


Fig. 4 Calculated (AM1, pseudoatom used instead of K^+) relative energies of 6579 valinomycin- K^+ conformers; the 27 C_3 symmetric structures are marked by vertical red lines. The lowest-energy part is magnified.

solvent environment corresponds to the negligible polarity of the isopropyl residues.

The relative energies, Boltzmann populations, and isopropyl torsional angles calculated for four lowest-energy conformers are listed in Table 1 and 2 (see Table S4 for more conformers†). In comparison to the vacuum BPW91/6-31G** results only minor energy (Table 1) and torsional angle (not shown) changes are caused by the CPCM solvent correction. Conformer II has a higher energy than I, but its Boltzmann population is still high because of the three-fold degeneracy enabled by its non-symmetrical geometry. Conformer I was confirmed in CDCl₃ solutions by NMR;⁶ the non-symmetric structures cannot be detected by NMR as discussed below. It is also interesting that the lowest-energy totally symmetric structure (I) differs from that found in a crystal of the C2221 space group grown in the presence of KI₅.¹³ This X-ray structure corresponds to conformer IV, the relative energy of which, however, makes its presence in solution improbable. The other X-ray geometry listed in Table 2, obtained in the presence of picrate anion and xylene in the crystals of the P2₁ space group,⁵ corresponds to a form that is even less populated in solution, at least according to the calculated energy of the corresponding conformer (3 kcal mol⁻¹, conformer number 8 in Table S4).† We suppose that this form is not present in solution because of the absence of the picrate interacting strongly with the complex in the crystal.⁵ Both the calculated and the crystal torsional angles significantly differ from the canonical values (−60, 60, 180°), which again suggests high flexibility of the molecule and, in the case of the solid state, significant influence of the crystal forces on the structure.

To estimate the role of the methanol solvent, the solvent probability distribution and position were analyzed in random MD snapshots (Fig. S7 and S8 in the ESI).† The analysis confirmed that the access of the solvent to the polar valinomycin groups is quite limited in the complex, to six carboxyl oxygen atoms. This corresponds to a relatively minor influence of the solvent on the relative conformer energies (Table 1). Moreover, even the hydrogen-bonded methanol positions change during the simulation (Fig. S8),† which presumably further limits the influence on the spectra including an induced solvent chirality, discussed previously for the vibrational optical activity of water complexes.⁸⁵

Calculated Raman and ROA spectra

Individual conformers provide relatively similar Raman scattering, but their ROA spectra differ in many features.

Table 2 Calculated (BPW91/6-31G**) torsion angles of the isopropyl groups in the K⁺-valinomycin complex conformers in Table 1

Conformer	L-Val	D-Hiv	D-Val
Calc.			
I	173	66	−173
	173	66	−173
	173	66	−173
II	173	66	173
	173	−67	−172
	173	66	−173
III	173	−67	−173
	172	−67	−172
	173	66	−173
IV	173	66	−173
	173	65	−173
	173	−178	−173
Exp.			
Ref. 13, X-ray “VALINK”	174	89	−177
	177	60	−176
	178	−124	−172
Ref. 5, X-ray “VALKPC10”	−178	175	−178
	179	169	−177
	175	176	−176
Ref. 6 NMR	180	60	180

This is documented on the calculated spectra of conformers I–III in Fig. 5. As the most apparent example, the intense ROA bands at the extended amide III region (around 1330 cm⁻¹) of

Table 1 Relative energies and populations of the three lowest-energy conformers of the K⁺-valinomycin complex

Conf.	<i>E</i> /kcal mol ⁻¹						<i>p</i> (%)		
	BPW91/6-31G**	BPW91/6-31G** ^a	B3PW91/6-31G**	B3LYP/6-31G**	B3LYP/6-311++G**		Calc. ^b	Exp. ^c	Exp. ^d
I	0	0	0	0	0		43	43	33
II	0.8	0.6	0.8	0.7	0.9		34	51	54
III	1.5	1.1	1.5	1.5	1.6		11	6	12
IV	1.4	1.3	1.4	1.2	1.5		12	0	0

^a CPCM solvent correction (methanol). ^b From the BPW91/6-31G**^a energies. ^c From the decomposition of experimental ROA spectrum into scaled calculated (B3LYP/6-31++G**/CPCM(MeOH)) subspectra. ^d Same as^c, but for calculated (B3PW91/6-31++G**/CPCM(MeOH)) subspectra (Fig. S9 in SI).

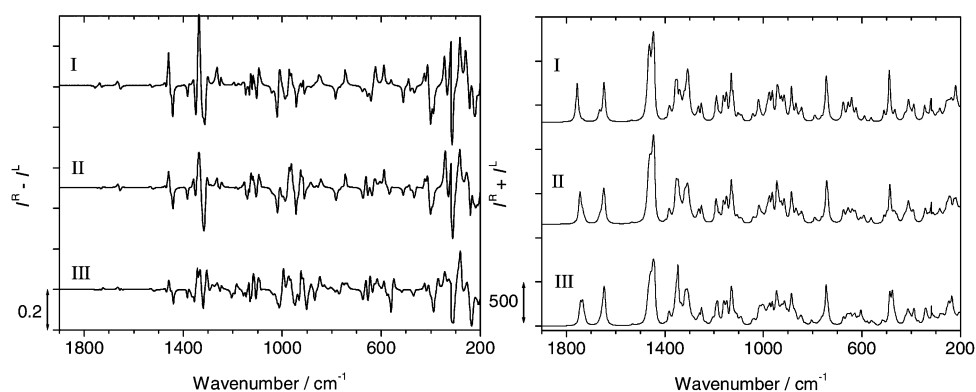


Fig. 5 Calculated ROA (left) and Raman (right) spectra (B3LYP/6-31++G**/CPCM/HF/6-31G**, see text) of three most-populated K^+ -valinomycin conformers.

conformers I and II are significantly reduced for conformer III. Note that these bands mark the formation of the complex in the experimental spectra (Fig. 3). Thus we can see that proper modeling of the side chains is necessary to accurately interpret the complexation changes. The ROA spectrum of conformer I is the closest to the experimentally observed shape.

Modern DFT functionals provide molecular force fields that lead to reliable spectral simulations.⁸⁶ This was also observed for the valinomycin complex, the Raman spectra of which were calculated at the BP86/SVP, BPW91/6-31G**, BPW91/CPCM/6-31G**, and B3LYP/CPCM/6-31++G** levels (Fig. 6). The GGA⁸⁷ BP86⁸⁸ functional provides rather underestimated frequencies of most vibrational bands, in comparison with the experiment. This can be partially corrected by the BPW91 method, also belonging to the GGA family. The CPCM

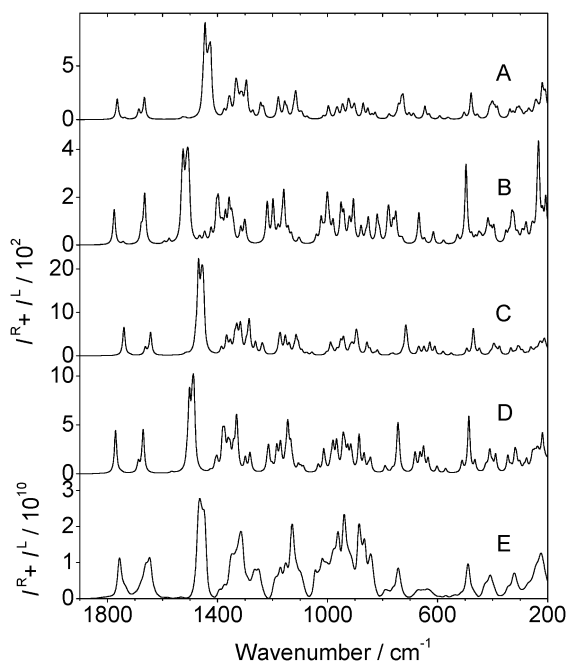


Fig. 6 Calculated (BP86/SVP (A), BPW91/6-31G** (B), BPW91/6-31G**/CPCM (C), and B3LYP/6-31++G**/CPCM (D), conformer I) and experimental (E) Raman spectra of the K^+ -valinomycin complex.

solvent correction leads to an intensity increase of many bands in the low-frequency region ($<1000\text{ cm}^{-1}$). As expected, the presumably more advanced B3LYP functional gives the best agreement. In addition, the correct B3LYP intensity profile within $800\text{--}1000\text{ cm}^{-1}$ range is only approximately matched by BPW91. Thus, although the BPW91 method was previously recommended for computations of peptide VCD^{89–92} and magnetic constants requiring correct spin densities,⁹³ the hybrid B3LYP functional appears more reliable for Raman simulation within a broader spectral region.

Neither was a particular advantage over B3LYP observed when the newer functionals were used for calculations of the Raman spectra of the L-Lac-L-Val-D-Hiv-D-Val- K^+ fragment. Very similar spectra profiles (*cf.* Fig. S6 of the ESI,[†] for M05 and M06) were obtained within $170\text{--}1600\text{ cm}^{-1}$. From Table S5,[†] where spectral and frequency errors are compiled for the B3LYP, M05, M06, M06L, M062X and B3LYP functionals, we can see that the B3LYP method provides the best results in the shortest computational time. The largest frequency variations exhibited the C=O stretching bands, which were typically calculated too high. The B3PW91 hybrid method (*cf.* Fig. S9) also provided valinomycin Raman and ROA spectra quite similar to those obtained by B3LYP.

In accord with previous studies^{32,38,45,94} the relatively small basis set used in the calculation of the ROA tensors for the whole molecule (larger basis sets were not affordable due to computational cost) seems to be sufficient for reliable spectra simulations, provided that the force field and the polarizability (α , and its reducible contributions to A and G)^{14,20} are accurate enough. Indeed, the 3-21G, 6-31G and 6-31G** basis sets used for ROA gave rather negligible differences in the simulated spectra (*cf.* Fig. S3).

Algebraic decomposition of the experimental spectrum into calculated sub-spectra

To obtain a more quantitative information about the conformer content of the complex, the scaled simulated spectra of conformers I, II and III were used in a mean square-root decomposition^{14,38} of the experimental ROA spectrum. As expected from the visual similarity of calculated spectral shapes of conformers I and II to the experimental ROA (*cf.* Fig. 3 and 5), populations of these two forms dominate (43 and 51% for the B3LYP functional, see Table 1), while the

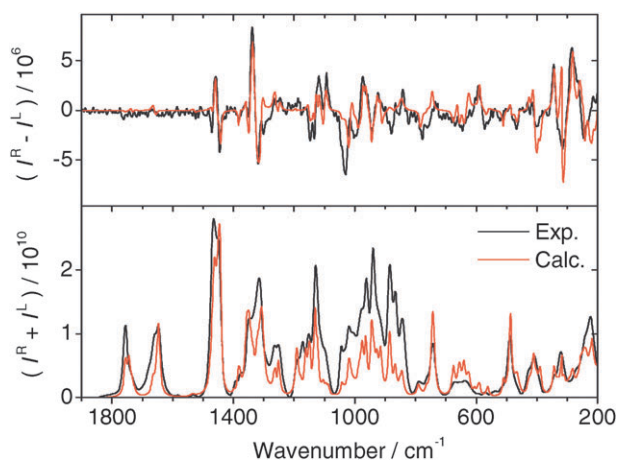


Fig. 7 The fitted (red, based on the B3LYP/6-31++G**/CPCM(MeOH)/HF/6-31G** conformer sub-spectra) and experimental (black) ROA (top) and Raman (bottom) spectra of the K^+ -valinomycin complex.

contribution of conformer III (6%) is on the brink of the decomposition error. Similar numbers (33, 54 and 12%) were obtained with the B3PW91 functional. The populations agree very well with the Boltzmann populations estimated from the calculated conformer energies. Note, however, that the Boltzmann factors are strongly dependent on the temperature; for low temperatures the population of I increases.

The decomposition coefficients were quite stable under minor variations of the fitting algorithm.¹⁴ For a two-spectrum fit, for example, we obtained a similar ratio of 40 and 60% to I and II, respectively. The higher probability of II seems to contradict the NMR experiment, where the form I was determined to be the prevalent conformer.⁶ However, one has to realize that even with the 40/60 I to II ratio, 80% of the D-Hiv residues still adopt the same angle ($\sim +60^\circ$). The conformation II which differs from I by only a single dihedral at Hiv (Table 2) is thus virtually invisible to NMR, while very distinct changes are observed in the ROA signal (*cf.* Fig. 5).

The resultant fitted ROA and Raman B3LYP spectra obtained from the three-conformer (I + II + III) decomposition are compared to the experimental ones in Fig. 7 (Fig. S9 for the B3PW91 functional).[†] Unlike the raw one-conformer spectrum (Fig. 5) excellent agreement of the calculated and experimental ROA and Raman spectra was achieved by the decomposition combined with the frequency scaling. The scaling introduces some error dependent on the band assignment; however, the uncertainty is small.¹⁴ Note that the conformer content is thus primarily obtained from calculated intensities that are more sensitive to the molecular shape than the frequencies.¹⁴ Minor deviations between the experimental and fitted spectra can be attributed to errors in the DFT force field and intensity tensors,⁸⁶ and to the approximations used for the solvent.^{38,53}

The experimental negative ROA signal at 1470 cm^{-1} is reproduced with negligible intensity only; its magnitude was found to depend strongly on fine parameters of the CCT transfer.⁴⁰ The Raman signal within $800\text{--}1600\text{ cm}^{-1}$ is dominated by many vibrations (CH bending, C–C stretching, *etc.*, see Table S1[†]) of the isopropyl residues, and it is impossible to assign individual

peaks. The overall Raman and ROA pattern is very well reproduced by the calculation, although the negative ROA signals at 1029 and 879 cm^{-1} are strongly underestimated. The low-frequency signal ($<600\text{ cm}^{-1}$), for polar molecules typically affected by the participation of attached solvent molecules from the first solvation shell,²⁸ seems to be reasonably well reproduced by the calculation with the implicit solvent for the hydrophobic valinomycin.

The effect of the isopropyl group dynamics on the spectra

The possibility of monitoring molecular flexibility by the inhomogeneous broadening of Raman and ROA spectral lines has been discussed for simpler aminoacids.^{27,28} As can be documented by the analysis of the MD trajectories of the valinomycin–potassium complex the torsion angles determining the positions of the isopropyl residues significantly oscillate around the equilibrium positions (the widths of the probability peaks are about 25° , see Fig. S4[†]). It is therefore desirable to at least qualitatively estimate the influence of this motion on the spectra. As can be seen on the 21 MD snapshot average (Fig. 8) the dynamical averaging does not significantly change the ROA and Raman intensity pattern, which indicates relative rigidity of the complex backbone as discussed above (Fig. 3). However, finer spectral features are influenced. For example, the relative intensities of the $1465/1450\text{ cm}^{-1}$ close Raman bands are switched by the averaging, in favor of the agreement with experiment. Within $600\text{--}800\text{ cm}^{-1}$ the one-conformer Raman spectra seem to be more realistic, while below 600 cm^{-1} better profile is obtained with the averaging. For ROA, the dynamical averaging is very beneficial for the signal within $400\text{--}650\text{ cm}^{-1}$; in other regions the one-conformer spectra appear more reliable, due to the limited precision of the simulations. Thus, we can conclude that the molecular motion is important for accurate spectral profiles, but its modeling is difficult due to the approximations used, and perhaps also due to the neglecting of quantum vibrational effects.^{81,95}

The locality and distance-dependence of the vibrational interactions

In order to better understand the dependence of the spectral signal on molecular structure, we selected two close and two distant valinomycin residues containing the isopropyl groups (Fig. 9), optimized the higher frequency-modes by the constrained normal mode optimization, and calculated the ROA and Raman spectra. The simpler HF/3-21G level was used for this computational experiment, with the polarization model used for the ROA intensities. As can be seen in Fig. 9, the interaction of the two close fragments separated by $\sim 5.4\text{ \AA}$ significantly contributes to the ROA intensities, and the resultant spectrum differs from that obtained as a plain sum of both residues. In particular, many ROA bands within $1400\text{--}1600\text{ cm}^{-1}$ change their signs as a result of the through-space coupling. Raman spectral changes are less apparent as they predominantly consist of peak frequency shifts. For the more distant fragments separated by $\sim 8.9\text{ \AA}$ (see the right hand side of Fig. 9) the spectra can be obtained without a significant loss of accuracy as sums of isolated residues.

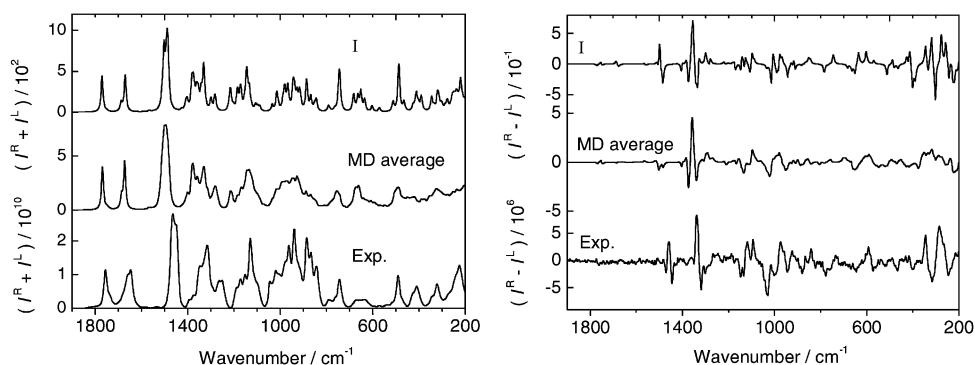


Fig. 8 Calculated Raman and ROA spectra of conformer I (top, 5 cm^{-1} bandwidth), averaged spectra from 21 MD snapshots (middle, 2 cm^{-1} bandwidth), and experimental spectra (bottom) for the K^+ -valinomycin complex. The calculated spectra were simulated with 5 and 2 cm^{-1} bandwidths for the one and multiple conformer simulations, respectively.

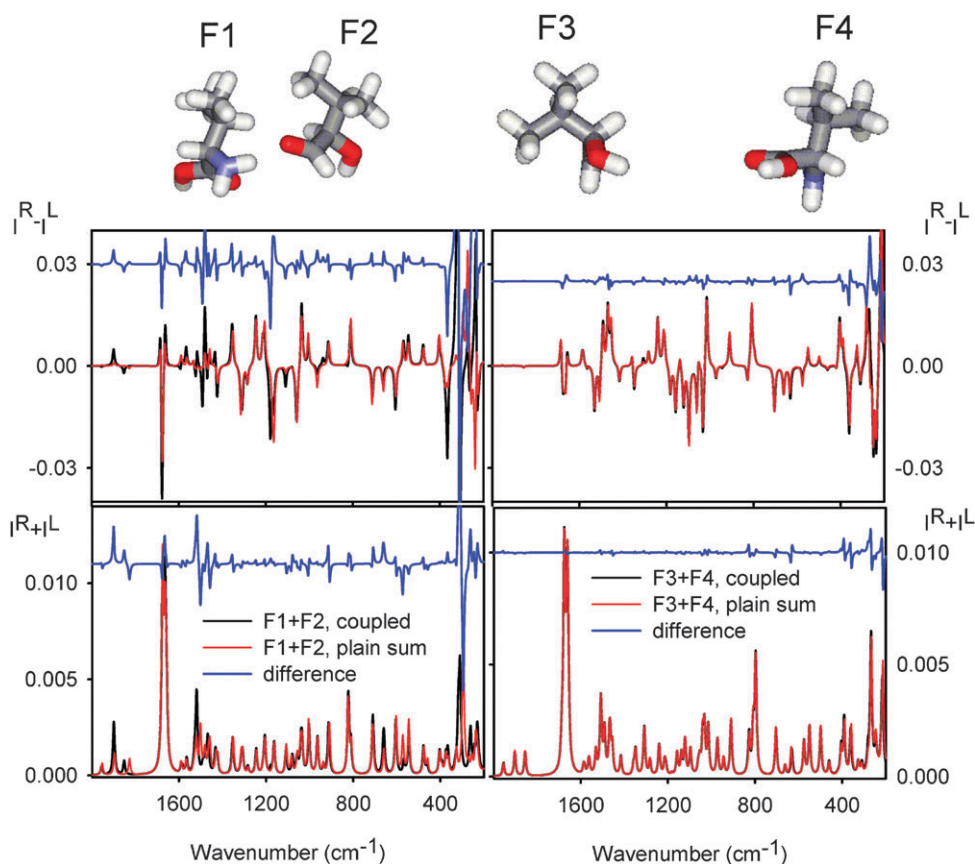


Fig. 9 Distance dependence of the through-space interaction: (top) ROA and (bottom) Raman (bottom) simulated (HF/3-21G) for two close (F1, F2, left, $^{\alpha}\text{C}$ - $^{\alpha}\text{C}$ distance is 5.4 \AA) and two more separated (F3, F4, right, $d(^{\alpha}\text{C}-^{\alpha}\text{C}) = 8.9 \text{ \AA}$) valinomycin residues.

This reflects the multipolar interactions that quickly decay with the distance.^{20,96}

In the last computational experiment, we simulated ROA and Raman spectra of neighboring valinomycin residues with and without the amide covalent link (Fig. 10). In this case, the through bond coupling introduces significant redistribution of both ROA and Raman intensities, similarly as for VCD peptide spectra.^{24,90} These results suggest that the vibrational interactions are fairly local, spreading about over two aminoacid residues. In the case when the isopropyl side chains are

spatially close (Fig. 9), however, the ROA technique may also be sensitive also to the tertiary protein structure.

Conclusions

The complexation of valinomycin with the potassium cation was clearly identifiable due to the changes in the Raman and ROA spectra. The reduced flexibility of the valinomycin in the complex caused narrowing of spectral lines, in particular in the lowest-frequency region. The rigid intramolecular hydrogen

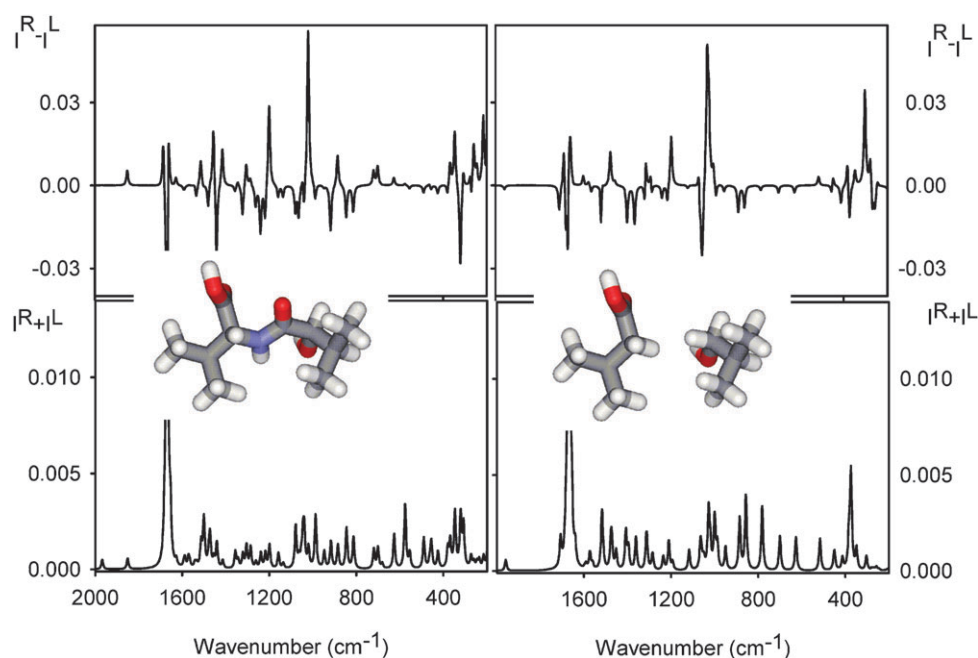


Fig. 10 The effect of through-bond coupling: (top) ROA and (bottom) Raman spectra calculated (HF/3-21G) for two valinomycin isopropyl residues with and without the amide linkage.

bond network was also accompanied, for example, by intensity changes of amide III and CH bending bands around 1300 cm^{-1} , and by a drop of the ROA peak at 879 cm^{-1} .

The rigidity of the complex made it more susceptible to accurate theoretical modeling. In particular, we could perform a full conformational search of the positions of the isopropyl side chains. The conformer populations thus obtained could be very well related to the experimental conformer ratios calculated from the algebraic decomposition of the experimental ROA spectra into calculated sub-spectra. The results were consistent with previous NMR studies; however, novel information about the presence of additional conformers in solution could be extracted.

The results thus document the exceptional sensitivity of ROA to the peptide side chain conformation that cannot be achieved by other optical spectroscopic techniques. A support of the ROA spectroscopy by the theoretical modeling is necessary for a reliable interpretation of the experimental data. In particular, the combination of high-precision DFT computational method, the Cartesian tensor transfer, and frequency scaling techniques enabled us to predict the conformer ratios of the K^+ -valinomycin complex in solution qualitatively. The sensitivity of the spectra to the molecular geometry confirmed the potential of ROA for structural studies of biomolecules.

Acknowledgements

The present study was undertaken owing to a support from the Academy of Sciences (grants A400550702, M200550902, and Z04 055 905), Czech Science Foundation (grant No. 203/09/2037), the Global COE Program Bio-Environmental Chemistry and ITP program of Osaka University (to S.Y.), European Reintegration Grant (No. 230955, to M.S.), and the Luna

(FZU), Metacentrum and University of Trømsø computer facilities. Special thanks are addressed to Prof. Werner Hug, University of Fribourg, who provided the necessary knowledge and equipment for the ROA measurement.

References

- 1 R. B. Gennis, *Biomembranes: Molecular Structure and Function*, Springer-Verlag, New York, 1989.
- 2 L. Stryer, *Biochemistry*, New York, 1995.
- 3 F. Wang, C. Zhao and P. L. Polavarapu, *Biopolymers*, 2004, **75**, 85–93.
- 4 L. Beven and H. Wroblewski, *Res. Microbiol.*, 1997, **148**, 163–175.
- 5 J. A. Hamilton, M. N. Sabesan and L. K. Steinrauf, *J. Am. Chem. Soc.*, 1981, **103**, 5880–5885.
- 6 V. F. Byistrov, Y. D. Gavrilov, V. T. Ivanov and Y. A. Ovchinnikov, *Eur. J. Biochem.*, 1977, **78**, 63–82.
- 7 M. M. Shemyakin, Y. A. Ovchinnikov, V. T. Ivanov, V. K. Antonov, E. I. Vinogradova, A. M. Shkrob, G. G. Malenkov, A. V. Evstratov, I. A. Laine, E. I. Melnik and I. D. Ryabova, *J. Membr. Biol.*, 1969, **1**, 402–430.
- 8 D. H. Haynes, A. Kowalsky and B. C. Pressman, *J. Biol. Chem.*, 1969, **244**, 502–505.
- 9 E. Grell, T. Funck and H. Sauter, *Eur. J. Biochem.*, 1973, **34**, 415–424.
- 10 D. F. Mayers and D. W. Urry, *J. Am. Chem. Soc.*, 1972, **94**, 77–81.
- 11 I. L. Karle, *J. Am. Chem. Soc.*, 1975, **97**, 4379–4386.
- 12 I. L. Karle and J. L. F. Anderson, *J. Am. Chem. Soc.*, 1988, **110**, 3253–3257.
- 13 K. Neupert-Laves and M. Dobler, *Helv. Chim. Acta*, 1975, **58**, 432–442.
- 14 M. Buděšínský, P. Daněček, L. Bednářová, J. Kapitán, V. Baumruk and P. Bouř, *J. Phys. Chem. A*, 2008, **112**, 8633–8640.
- 15 I. M. Asher, K. J. Rothschild and H. E. Stanley, *J. Mol. Biol.*, 1974, **89**, 205–222.
- 16 W. K. Liddle, T. W. Willis, A. T. Tu, M. B. Sankaram, S. Devarajan and K. R. K. Easwaran, *Chem. Phys. Lipids*, 1985, **36**, 303–308.
- 17 I. M. Asher, K. J. Rothschild, E. Anastassakis and H. E. Stanley, *J. Am. Chem. Soc.*, 1977, **99**, 2024–2032.
- 18 K. J. Rothschild, I. M. Asher, H. E. Stanley and E. Anastassakis, *J. Am. Chem. Soc.*, 1977, **99**, 2032–2039.

- 19 C. A. Hasselbacher and T. G. Dewey, *Photosynth. Res.*, 1986, **8**, 79–86.
- 20 L. D. Barron, *Molecular Light Scattering and Optical Activity*, Cambridge University Press, Cambridge, 2004.
- 21 L. D. Barron, M. P. Bogaard and A. D. Buckingham, *J. Am. Chem. Soc.*, 1973, **95**, 603–605.
- 22 T. A. Keiderling, in *Infrared and Raman Spectroscopy of Biological Materials*, ed. B. Yan and H. U. Gremlich, M. Dekker, New York, 1999.
- 23 W. C. Johnson, *Proteins: Struct., Funct., Genet.*, 1990, **7**, 205–214.
- 24 P. Bouř and T. A. Keiderling, *J. Am. Chem. Soc.*, 1993, **115**, 9602–9607.
- 25 P. Mukhopadhyay, G. Zuber and D. N. Beratan, *Biophys. J.*, 2008, **95**, 5574–5586.
- 26 R. A. G. D. Silva, J. Kubelka, S. M. Decatur, P. Bouř and T. A. Keiderling, *Proc. Natl. Acad. Sci. U. S. A.*, 2000, **97**, 8318–8323.
- 27 J. Kapitán, V. Baumruk, V. Kopecký, Jr. and P. Bouř, *J. Phys. Chem. A*, 2006, **110**, 4689–4696.
- 28 J. Kapitán, V. Baumruk, V. Kopecký, Jr., R. Pohl and P. Bouř, *J. Am. Chem. Soc.*, 2006, **128**, 13451–13462.
- 29 J. Haesler, I. Schindelholz, E. Riguet, C. G. Bochet and W. Hug, *Nature*, 2007, **446**, 526–529.
- 30 J. Kaminský, J. Kapitán, V. Baumruk, L. Bednářová and P. Bouř, *J. Phys. Chem. A*, 2009, **113**, 3594–3601.
- 31 T. Helgaker, K. Ruud, K. L. Bak, P. Joergensen and J. Olsen, *Faraday Discuss.*, 1994, **99**, 165–180.
- 32 K. Ruud, T. Helgaker and P. Bouř, *J. Phys. Chem. A*, 2002, **106**, 7448–7455.
- 33 J. R. Cheeseman, *Calculation of Molecular Chiroptical Properties Using Density Functional Theory*, CD 2007, Groningen, 2007.
- 34 V. Liegeois, K. Ruud and B. Champagne, *J. Chem. Phys.*, 2007, **127**, 204105.
- 35 M. J. Frisch, G. W. Trucks, H. B. Schlegel, G. E. Scuseria, M. A. Robb, J. R. Cheeseman, G. Scalmani, V. Barone, B. Mennucci, G. A. Petersson, H. Nakatsuji, M. Caricato, X. Li, H. P. Hratchian, A. F. Izmaylov, J. Bloino, G. Zheng, J. L. Sonnenberg, M. Hada, M. Ehara, K. Toyota, R. Fukuda, J. Hasegawa, M. Ishida, T. Nakajima, Y. Honda, O. Kitao, H. Nakai, T. Vreven, J. Montgomery, J. A., J. E. Peralta, F. Ogliaro, M. Bearpark, J. J. Heyd, E. Brothers, K. N. Kudin, V. N. Staroverov, R. Kobayashi, J. Normand, K. Raghavachari, A. Rendell, J. C. Burant, S. S. Iyengar, J. Tomasi, M. Cossi, N. Rega, J. M. Millam, M. Klene, J. E. Knox, J. B. Cross, V. Bakken, C. Adamo, J. Jaramillo, R. Gomperts, R. E. Stratmann, O. Yazyev, A. J. Austin, R. Cammi, C. Pomelli, J. W. Ochterski, R. L. Martin, K. Morokuma, V. G. Zakrzewski, G. A. Voth, P. Salvador, J. J. Dannenberg, S. Dapprich, A. D. Daniels, O. Farkas, J. B. Foresman, J. V. Ortiz, J. Cioslowski and D. J. Fox, Gaussian, Inc., Wallingford CT, 2009.
- 36 C. Angeli, K. L. Bak, V. Bakken, O. Christiansen, R. Cimraglia, S. Coriani, P. Dahle, E. K. Dalskov, T. Enevoldsen, B. Fernandez, C. Haettig, K. Hald, A. Halkier, H. Heiberg, T. Helgaker, H. Hettema, H. J. A. Jensen, D. Jonsson, P. Joergensen, S. Kirpekar, W. Klopper, R. Kobayashi, H. Koch, O. B. Lutnaes, K. V. Mikkelsen, P. Norman, J. Olsen, M. J. Packer, T. B. Pedersen, Z. Rinkevicius, E. Rudberg, T. A. Ruden, K. Ruud, P. Salek, A. Sanchez de Meras, T. Saue, S. P. A. Sauer, B. Schimmelpfennig, K. O. Sylvester-Hvid, P. R. Taylor, O. Vahtras, D. J. Wilson and H. Agren, *University of Oslo*, Oslo, Release 2.0 edn, 2005–2009.
- 37 M. Reiher, V. Liegeois and K. Ruud, *J. Phys. Chem. A*, 2005, **109**, 7567–7574.
- 38 J. Šebek, J. Kapitán, J. Šebestík, V. Baumruk and P. Bouř, *J. Phys. Chem. A*, 2009, **113**, 7760–7768.
- 39 C. Herrmann, K. Ruud and M. Reiher, *ChemPhysChem*, 2006, **7**, 2189–2196.
- 40 P. Bouř, J. Sopková, L. Bednářová, P. Maloň and T. A. Keiderling, *J. Comput. Chem.*, 1997, **18**, 646–659.
- 41 P. Bouř and T. A. Keiderling, *J. Phys. Chem. B*, 2005, **109**, 23687–23697.
- 42 J. Kubelka, P. Bouř and T. A. Keiderling, in *Advances in Biomedical Spectroscopy, Biological and Biomedical Infrared Spectroscopy*, ed. A. Barth and P. I. Haris, IOS Press, Amsterdam, 2009, vol. 2, pp. 178–223.
- 43 J. Kubelka and T. A. Keiderling, *J. Am. Chem. Soc.*, 2001, **123**, 12048–12058.
- 44 V. Andrushchenko, H. Wieser and P. Bouř, *J. Phys. Chem. B*, 2002, **106**, 12623–12634.
- 45 J. Kapitán, V. Baumruk, V. Kopecký, Jr. and P. Bouř, *J. Am. Chem. Soc.*, 2006, **128**, 2438–2443.
- 46 P. Bouř, *J. Comput. Chem.*, 2001, **22**, 426–435.
- 47 P. Bouř and T. A. Keiderling, *J. Chem. Phys.*, 2002, **117**, 4126–4132.
- 48 P. Bouř, *Collect. Czech. Chem. Commun.*, 2005, **70**, 1315–1340.
- 49 V. Andrushchenko and P. Bouř, *J. Phys. Chem. A*, 2007, **111**, 9714–9723.
- 50 P. Bouř, J. Kim, J. Kapitán, R. P. Hamer, R. Juany, L. Wu and T. A. Keiderling, *Chirality*, 2008, **20**, 1104–1119.
- 51 A. Klamt, in *The Encyclopedia of Computational Chemistry*, ed. P. R. Schleyer, N. L. Allinger, T. Clark, J. Gasteiger, P. A. Kollman, H. F. Schaefer III and P. R. Schreiner, John Wiley & Sons, Chichester, 1998, vol. 1, pp. 604–615.
- 52 K. J. Jalkanen, R. M. Nieminen, M. Knapp-Mohammady and S. Suhai, *Int. J. Quantum Chem.*, 2003, **92**, 239–259.
- 53 K. J. Jalkanen, R. M. Nieminen, K. Frimand, J. Bohr, H. Bohr, R. C. Wade, E. Tajkhorshid and S. Suhai, *Chem. Phys.*, 2001, **265**, 125–151.
- 54 P. Bouř, D. Michalík and J. Kapitán, *J. Chem. Phys.*, 2005, **122**, 144501.
- 55 P. Bouř, *J. Chem. Phys.*, 2004, **121**, 7545–7548.
- 56 S. Abdali, K. J. Jalkanen, H. Bohr, S. Suhai and R. M. Nieminen, *Chem. Phys.*, 2002, **282**, 219–235.
- 57 E. Tajkhorshid, K. J. Jalkanen and S. Suhai, *J. Phys. Chem. B*, 1998, **102**, 5899–5913.
- 58 E. Deplazes, W. vanBronswijk, F. Zhu, L. D. Barron, S. Ma, L. A. Nafie and K. J. Jalkanen, *Theor. Chem. Acc.*, 2008, **119**, 155–176.
- 59 W. Hug and G. Hangartner, *J. Raman Spectrosc.*, 1999, **30**, 841–852.
- 60 W. Hug, *Appl. Spectrosc.*, 2003, **57**, 1–13.
- 61 P. Bouř and P. Maloň, *Academy of Sciences*, Prague, 1995–2009.
- 62 J. P. P. Stewart, in *The Encyclopedia of Computational Chemistry*, ed. P. R. Schleyer, N. L. Allinger, T. Clark, J. Gasteiger, P. A. Kollman, H. F. Schaefer III and P. R. Schreiner, John Wiley & Sons, Chichester, 1998, vol. 2, pp. 2080–2086.
- 63 M. J. S. Dewar, E. G. Zoebisch and E. F. Healy, *J. Am. Chem. Soc.*, 1985, **107**.
- 64 A. Becke, *Phys. Rev. A: At., Mol., Opt. Phys.*, 1988, **38**, 3098–3100.
- 65 A. D. Becke, *J. Chem. Phys.*, 1993, **98**, 5648–5652.
- 66 J. P. Perdew, K. Burke and Y. Wang, *Phys. Rev. B: Condens. Matter*, 1996, **54**, 16533–16539.
- 67 S. Grimme, *J. Comput. Chem.*, 2004, **25**, 1463–1473.
- 68 T. Schwabe and S. Grimme, *Phys. Chem. Chem. Phys.*, 2007, **9**, 3397–3406.
- 69 V. Parchaňský, P. Matějka, B. Dolenský, M. Havlík and P. Bouř, *J. Mol. Struct.*, 2009, **934**, 117–122.
- 70 J. W. Ponder, Washington University School of Medicine, Saint Louis, 3.8 edn, 2000.
- 71 J. Wang, P. Cieplak and P. A. Kollman, *J. Comput. Chem.*, 2000, **21**, 1049–1074.
- 72 R. Ahlrichs, M. Bar, H.-P. Baron, R. Bauernschmitt, S. Bocker, M. Ehrig, K. Eichkorn, S. Elliot, F. Furche, F. Haase, M. Haser, H. Horn, C. Huber, U. Huniar, M. Kattannek, C. Kolmel, M. Koolwitz, K. May, C. Ochsenfeld, H. Ohm, A. Schafer, U. Schneider, O. Treutler, M. von Arnim, F. Weigend, P. Weiss and H. Weiss, *Quantum Chemistry Group*, University of Karlsruhe, Karlsruhe, 1998.
- 73 Y. Zhao, N. E. Schultz and D. G. Truhlar, *J. Chem. Phys.*, 2005, **123**, 161103.
- 74 Y. Zhao and D. G. Truhlar, *Theor. Chem. Acc.*, 2008, **120**, 215–241.
- 75 Y. Zhao and D. G. Truhlar, *J. Phys. Chem. A*, 2006, **110**, 13126–13130.
- 76 P. Bouř, Academy of Sciences, Prague, 1997–2009.
- 77 P. L. Polavarapu, *Vibrational Spectra and Structure*, 1984, **13**, 103–160.
- 78 L. A. Nafie, in *Modern Nonlinear Optics, Part 3*, ed. M. Evans and S. Kielich, Wiley, New York, 1994, vol. 85, pp. 105–206.
- 79 P. Bouř, Academy of Sciences, Prague, 1994–2009.

- 80 M. Buděšínský, J. Šebestík, L. Bednářová, V. Baumruk, M. Šafařík and P. Bouř, *J. Org. Chem.*, 2008, **73**, 1481–1489.
- 81 J. Kapitán, L. Hecht and P. Bouř, *Phys. Chem. Chem. Phys.*, 2008, **10**, 1003–1008.
- 82 J. Kaminský, J. Šebek and P. Bouř, *J. Comput. Chem.*, 2009, **30**, 983–991.
- 83 M. Diem, *Introduction to Modern Vibrational Spectroscopy*, Wiley, New York, 1993.
- 84 L. D. Barron, L. Hecht, E. W. Blanch and A. F. Bell, *Prog. Biophys. Mol. Biol.*, 2000, **73**, 1–49.
- 85 M. Losada and Y. Xu, *Phys. Chem. Chem. Phys.*, 2007, **9**, 3127–3135.
- 86 P. Daněček, J. Kapitán, V. Baumruk, L. Bednářová, V. Kopecký, Jr. and P. Bouř, *J. Chem. Phys.*, 2007, **126**, 224513.
- 87 R. G. Parr and W. Yang, *Density-functional Theory of Atoms and Molecules*, Oxford University Press, New York, 1994.
- 88 J. P. Perdew, *Phys. Rev. B: Condens. Matter*, 1986, **33**, 8822–8824.
- 89 R. Huang, J. Kubelka, W. Barber-Armstrong, R. A. G. D. Silva, S. M. Decatur and T. A. Keiderling, *J. Am. Chem. Soc.*, 2004, **126**, 2346–2354.
- 90 J. Kubelka, R. A. G. D. Silva and T. A. Keiderling, *J. Am. Chem. Soc.*, 2002, **124**, 5325–5332.
- 91 J. Hilario, J. Kubelka, F. A. Syud, S. H. Gellman and T. A. Keiderling, *Biospectroscopy*, 2002, **67**, 233–236.
- 92 P. Bouř, J. Kubelka and T. A. Keiderling, *Biopolymers*, 2002, **65**, 45–69.
- 93 M. Filatov and D. Cremer, *J. Chem. Phys.*, 2005, **123**, 124101.
- 94 M. Pecul and K. Ruud, *Int. J. Quantum Chem.*, 2005, **104**, 816–829.
- 95 V. Andrushchenko, P. Matějka, D. T. Anderson, J. Kaminský, J. Horníček, L. O. Paulson and P. Bouř, *J. Phys. Chem. A*, 2009, **113**, 9727–9736.
- 96 P. Bouř and T. A. Keiderling, *J. Am. Chem. Soc.*, 1992, **114**, 9100–9105.